Center for Turbulence Research
Proceedings of the Summer Program 2006

Transition to turbulence in MHD channel flow with spanwise magnetic field

By T. Boeck†, D. Krasnov†, M. Rossi‡, O. Zikanov¶ AND B. Knaepen‖

We investigate the linear and non-linear evolution of perturbations in a magnetohydrodynamic channel flow with electrically insulating channel walls in which a strong magnetic field possesses an orientation orthogonal to the stream but parallel to the walls. Linear optimal perturbations and their maximum amplifications over finite time intervals are computed using an iterative scheme based on the direct and adjoint governing equations. We find that the presence of a magnetic field changes the spatial structure of optimal perturbations. As the Hartmann number increases, the optimal modes cease to be the classical streamwise rolls and become oblique rolls with axes at some angle to the direction of the flow. At sufficiently high Hartmann numbers, the optimal modes are purely spanwise Tollmien-Schlichting waves. For certain Reynolds and Hartmann numbers, direct numerical simulations are performed to investigate how the transition to turbulence is affected by the magnetic field. Simulations are conducted using the optimal modes as initial values with weak three-dimensional noise added at the beginning or at maximum amplification time.

1. Introduction

In this paper we consider the transition to turbulence in a pressure-driven flow of an electrically conducting fluid within a plane channel. The flow is affected by a steady uniform magnetic field imposed in the spanwise (parallel to the wall and perpendicular to the flow) direction. We show that, while leaving the basic velocity profile unchanged, the magnetic field can dramatically transform the evolution of unstable perturbations and the transition to turbulence.

A channel flow in a purely spanwise magnetic field, although an idealization, can be viewed as a generalized model of flows in the presence of a magnetic field with non-zero component parallel to solid walls. Such flows can be found in numerous metallurgical and materials processing applications. Prominent examples include, among others, the electromagnetic flow control in continuous steel casting (Davidson 1999; Thomas & Zhang 2001) and in growth of large silicon crystals (von Ammon *et al.* 2005). Another area of application is the liquid metal (Li or Pb-17Li) cooling blankets of breeder type for fusion reactors (Barleon *et al.* 2001). The typical blanket design includes a duct flow in a strong imposed magnetic field. Instability and transition to turbulence in sidewall boundary layers (in respect to which the magnetic field is spanwise) is one of the possible ways to achieve the desired intensification of heat and mass transfer. The channel flow considered in this paper can be seen as a limiting case of a duct flow at a large aspect ratio. From a different application viewpoint, Lee and Choi (2001) have shown that a

† Ilmenau University of Technology
‡ University of Paris VI
¶ University of Michigan – Dearborn
‖ Université Libre de Bruxelles

spanwise magnetic field can lead to substantial reduction of the turbulent drag in a channel flow.

With regard to the general theory of instability and transition to turbulence in parallel shear flows, the situation of a channel in a spanwise field is of substantial interest. The applied magnetic field renders the spanwise direction preferable in the sense that the perturbations uniform in this direction are not directly affected, in particular, not suppressed, by the magnetic field. This results in a different symmetry of the problem and, as demonstrated in our paper, in remarkable new features of the transition.

Among the possible transition scenarios, we focus on the one based on the algebraic transient growth of optimal perturbations and their subsequent three-dimensional breakdown. This scenario was shown to realize in other parallel shear flows, such as the plane Poiseuille (Reddy *et al.* 1998), pipe Poiseuille (Zikanov 1996), and Hartmann (Krasnov *et al.* 2004) flows.

After formulating the problem in Section 2, we analyze the transient evolution of linear perturbations in Section 3. Note that, due to the effect of the spanwise magnetic field, arbitrary three-dimensional perturbations have to be considered in contrast to the classical non-magnetic case when the optimal perturbations are uniform in the streamwise direction. In Section 4, the non-linear evolution of the optimal modes, and the transition to turbulence triggered by superimposed three-dimensional noise are investigated in direct numerical simulations (DNS).

2. Problem formulation

We consider the flow of an incompressible electrically conducting fluid in an infinite plane channel between insulating walls located at $z = \pm d/2$, where x, y, and z denote the streamwise, spanwise, and vertical directions, respectively. The flow is driven by a pressure gradient $\partial P_0/\partial x$ in the x-direction and submitted to a constant spanwise magnetic field of strength $B_0 : \boldsymbol{B}_0 = B_0\boldsymbol{e}$ with $\boldsymbol{e} \equiv (0, 1, 0)$.

We assume that the magnetic Reynolds number $Re_m \equiv UL\sigma\mu$ is small. Here, U and L are the velocity and length scales to be defined below, σ is the electric conductivity of the fluid, and μ is the magnetic permittivity of the vacuum. In the limit $Re_m \ll 1$ we can apply the quasi-static approximation (Roberts 1967), whereby the fluctuations of the magnetic field arising due to the fluid motion adjust instantaneously to the velocity fluctuations and are much weaker than the imposed magnetic field. The governing equations reduce to the Navier-Stokes system with the additional Lorentz force:

$$\frac{\partial \boldsymbol{v}}{\partial t} + (\boldsymbol{v}\cdot\nabla)\boldsymbol{v} = -\frac{1}{\rho}\nabla p + \nu\nabla^2\boldsymbol{v} + \frac{1}{\rho}\left(\boldsymbol{j}\times\boldsymbol{B}_0\right), \tag{2.1}$$

$$\nabla\cdot\boldsymbol{v} = 0, \tag{2.2}$$

where ν and ρ stand for the kinematic viscosity and the density of the fluid. The induced electric current density is given by Ohm's law:

$$\boldsymbol{j} = \sigma\left(-\nabla\phi + \boldsymbol{v}\times\boldsymbol{B}_0\right). \tag{2.3}$$

Neglecting the displacement currents and assuming that the fluid is electrically neutral, we require that $\nabla\cdot\boldsymbol{j} = 0$. This leads to an equation for the electric potential ϕ:

$$\nabla^2\phi = \nabla\cdot\left(\boldsymbol{v}\times\boldsymbol{B}_0\right). \tag{2.4}$$

Periodicity conditions are used in the x- and y-directions following the assumption of

flow homogeneity. The no-slip conditions $\boldsymbol{v} = 0$ are imposed at the walls $z = \pm d/2$. The electric potential ϕ is also periodic in the x- and y-directions. Since no current flows through the electrically insulating walls and the velocity $\boldsymbol{v}$ is zero at these walls, (2.3) leads to $\partial\phi/\partial z = 0$ at $z = \pm d/2$.

It is important to stress that a uniform spanwise magnetic field does not affect the basic Poiseuille flow or any other flow with a velocity field independent of the spanwise coordinate. This can be easily verified by taking the *curl* of Ohm's law (2.3), which leads to

$$\nabla \times \boldsymbol{j} = \sigma(\boldsymbol{B} \cdot \nabla)\boldsymbol{v} = 0.$$

The only solution in the absence of externally imposed currents is $\boldsymbol{j} = 0$. A spanwise-uniform flow does not induce any currents and evolves in a purely hydrodynamic manner. The basic velocity field, thus, has the classical parabolic profile:

$$U_H(z) = -\frac{d^2}{8\nu\rho}\frac{\partial P_0}{\partial x}\left(1 - \frac{4z^2}{d^2}\right), \tag{2.5}$$

with the basic pressure field $P_H(x) = (\partial P_0/\partial x)x$. Finally, the basic electric potential reads

$$\phi_H(z) = -\frac{d^2 B_0}{8\nu\rho}\frac{\partial P_0}{\partial x}\left(z - \frac{4z^3}{3d^2}\right). \tag{2.6}$$

For non-dimensionalization, the Poiseuille flow centerline velocity is used as velocity scale U:

$$U \equiv -\frac{d^2}{8\nu\rho}\frac{\partial P_0}{\partial x}. \tag{2.7}$$

The characteristic length is taken to be the channel half width $L \equiv d/2$. The imposed magnetic field and the electric potential scale with B_0 and LUB_0, respectively. Finally, the units of time and pressure are taken as L/U and ρU^2. The non-dimensional basic velocity profile is

$$U_H(z) = 1 - z^2 \tag{2.8}$$

and the non-dimensional governing equations and boundary conditions are

$$\frac{\partial \boldsymbol{v}}{\partial t} + (\boldsymbol{v} \cdot \nabla)\boldsymbol{v} = -\nabla p + \frac{1}{Re}\nabla^2 \boldsymbol{v} + N\left(-\nabla\phi \times \boldsymbol{e} + (\boldsymbol{v} \times \boldsymbol{e}) \times \boldsymbol{e}\right), \tag{2.9}$$

$$\nabla \cdot \boldsymbol{v} = 0, \tag{2.10}$$

$$\nabla^2 \phi = \nabla \cdot (\boldsymbol{v} \times \boldsymbol{e}), \tag{2.11}$$

$$v_x = v_y = v_z = \frac{\partial \phi}{\partial z} = 0 \quad \text{at } z = \pm 1. \tag{2.12}$$

The non-dimensional parameters are the Reynolds number

$$Re = \frac{[U][L]}{\nu} = -\frac{d^3}{16\nu^2\rho}\frac{\partial P_0}{\partial x}, \tag{2.13}$$

and one of the MHD parameters, either the Hartmann number

$$Ha = \frac{B_0 d}{2}\sqrt{\frac{\sigma}{\rho\nu}} \tag{2.14}$$

or the magnetic interaction parameter $N \equiv Ha^2/Re$. Finally, we assume that the volume flux Q per span width is constant in the DNS.

3. Linear perturbations

The flow fields are now considered as split into a basic flow (2.8) and three-dimensional perturbations:

$$\boldsymbol{v} = U_H(z)(1,0,0) + \boldsymbol{v}_p, \quad \phi = \phi_H(z) + \phi_p(x,y,z), \quad p = P_H(z) + p_p. \tag{3.1}$$

We linearize the system (2.9–2.12) with respect to the perturbations, and consider the evolution of decoupled monochromatic Fourier modes

$$(\boldsymbol{v}_p, \phi_p, p_p) = (\hat{u}(z,t), \hat{v}(z,t), \hat{w}(z,t), \hat{\phi}(z,t), \hat{p}(z,t)) \exp(i\alpha x + i\beta y), \tag{3.2}$$

where α and β are the wavenumbers in the streamwise (x) and spanwise (y) directions.

In this study, we consider cases in which the flow is linearly stable, i.e., all eigensolutions decay exponentially. It is known from previous studies (see, e.g., Butler and Farrell 1992 or Reddy *et al.* 1998) that, due to the non-normality of the linear operator, the eigenmodes may form combinations that experience substantial transient algebraic growth before they eventually decay. We focus on such modes and consider their amplification with the prospect, further analyzed in Section 4, that transition to turbulence can be triggered by their non-linear evolution. To quantify the amplification at time T, a norm is to be defined, which is typically the kinetic energy of the perturbations. This norm can be orthogonally decomposed in a Fourier basis in the x and y directions, which implies that the individual contributions of each wavenumber pair (α, β) can be considered independently. We follow such a procedure and define the norm

$$E(T) \equiv \int (\hat{u}(z,T)\hat{u}^+(z,T) + \hat{v}(z,T)\hat{v}^+(z,T) + \hat{w}(z,T)\hat{w}^+(z,T))\mathrm{d}z \tag{3.3}$$

where the superscript + denotes complex conjugation. Spatial integration is performed over the entire channel width, and the perturbations are obtained by time integration of the governing equations over the time interval $[0,T]$.

The amplification gain of any given mode at time T is the ratio $E(T)/E(0)$. This ratio can be maximized over all possible initial vertical shapes in (3.2) to give the maximum amplification $\hat{G}(T,\alpha,\beta)$ of the disturbances with the wavenumbers (α,β) at the time T. The optimal perturbations providing the maximum amplification $\hat{G}(T,\alpha,\beta)$ are found by an optimization procedure (e.g., Farrell and Ioannou 1996; Schmid and Henningson 2000). We solve this problem with the help of a Lagrangian formalism in which Lagrangian multipliers are introduced to enforce the following constraints: (1) the disturbance energy at time $T = 0$ is equal to unity; (2) the disturbance satisfies the linear governing equation as well as the boundary conditions during the complete time interval $[0,T]$. In the present case, these multipliers are the adjoint fields

$$(\tilde{\boldsymbol{v}}, \tilde{\phi}, \tilde{p}) = (\tilde{u}(z,t), \tilde{v}(z,t), \tilde{w}(z,t), \tilde{\phi}(z,t), \tilde{p}(z,t)). \tag{3.4}$$

The optimal perturbation for time T is obtained through an iterative scheme. Each iteration consists of a forward and a backward integration. The forward integration propagates a given initial condition forward in time using the direct problem. The result serves as an "initial" condition for the backward integration from $t = T$ to $t = 0$ using the adjoint equations. After the full forward-backward integration, an updated initial condition for the next iterative step is available. Convergence is reached when the initial condition for the forward problem does not change appreciably – up to a normalization constant – from one iterative step to the next. The maximum energy amplification is then computed by propagating the converged initial condition forward in time and by forming the ratio

$E(T)/E(0)$. The direct and adjoint equations have been discretized using a pseudospectral scheme based on Chebyshev polynomials and a projection-like method to enforce the incompressibility.

In the present study we consider the Reynolds number $Re = 5000$, for which the non-magnetic case has been well studied (see Butler and Farrell 1992). The search for optimal perturbations is performed in a square (α,β)-domain with α and β varying in the range from 0 to 4. This domain was sufficient to capture the peaks of the maximum energy amplification except at small times T, where it is necessarily low. The number of Chebyshev polynomials used is 64. To ensure that this number of polynomials is sufficient we have verified all the maxima with 128 polynomials, with obtained differences being less than 1%.

The iterative method computes the maximum energy amplification $\hat{G}(T, \alpha, \beta, Ha, Re)$ for a given wavenumber pair (α, β) and a given time T. The function can be maximized over α, β, and T to provide the global maximum and the corresponding optimal mode at given Re and Ha. Alternatively, one can study perturbations of a certain symmetry, for example, the streamwise perturbations with $\alpha = 0$, or analyze the entire distribution in the (α, β) plane for different times T.

The latter approach is illustrated in Fig. 1 for the case $Ha = 50$ and $Re = 5000$. The contours indicate variation of $\hat{G}$ from low (white regions) to high (black regions) values. There are four snapshots corresponding to different moments in time T: (a) the moment of highest amplification $T \approx 15$, (b) the moment of three coexisting local maxima $T \approx 28$, (c) the moment $T \approx 33$ when the local maxima have merged into one global maximum, and (d) the moment $T \approx 88$ of appearance of a new local maximum. Note that, while the highest amplification in the non-magnetic case $Ha = 0$ is achieved by purely streamwise vortices with $\alpha = 0$ (Butler and Farrell 1992), the global maximum at $Ha = 50$ corresponds to a three-dimensional perturbation with α and β both non-zero.

The distribution $\hat{G}(T, \alpha, \beta)$ can be maximized over the (α, β)-plane at given T, which provides the maximum amplification $\hat{M}_{tot}(T)$, as well as the corresponding optimal wavenumbers $(\alpha_{opt}, \beta_{opt})$. In the same way, but limiting the consideration to $\alpha = 0$, we can determine the maximum amplification $\hat{M}_{stream}(T)$ and β_{stream} for purely streamwise perturbations. These quantities are displayed in Fig. 2 as a function of time T for the Reynolds number $Re = 5000$ and the three Hartmann numbers $Ha = 10$, 50, and 100.

First, we note that the effect of the magnetic field is already well pronounced at $Ha = 10$ (Fig. 2a). The maximum $\hat{M}_{tot}$ is observed for an oblique mode at $T \approx 64$, whereas streamwise modes provide a twice-smaller amplification $\hat{M}_{stream}$ much later at $T \approx 189$. For $Ha = 50$, the influence of the magnetic field becomes stronger as we observe three global maxima corresponding to different oblique modes, which appear long before the streamwise perturbations reach their maximum amplification. The situation at $Ha = 100$ collapses to only one family of dominant modes with $\alpha \neq 0$ and $\beta = 0$. These perturbations have the form of purely spanwise vortices (whose axes are parallel to the magnetic field).

The results of these and other computations conducted at smaller Ha numbers are summarized in Fig. 3, where the global (maximized over time) optimal modes are presented. The wavenumber vector (α_{opt},β_{opt}) turns toward the x-axis as the Hartmann number increases from 0 to 100 (see Fig. 3a). The optimal mode changes from streamwise vortices for $Ha = 0$ to three-dimensional (oblique) vortices at $Ha \geq 5$. The oblique angle increases with further growth of Ha, until the purely spanwise vortices become dominant at $Ha \geq 100$.

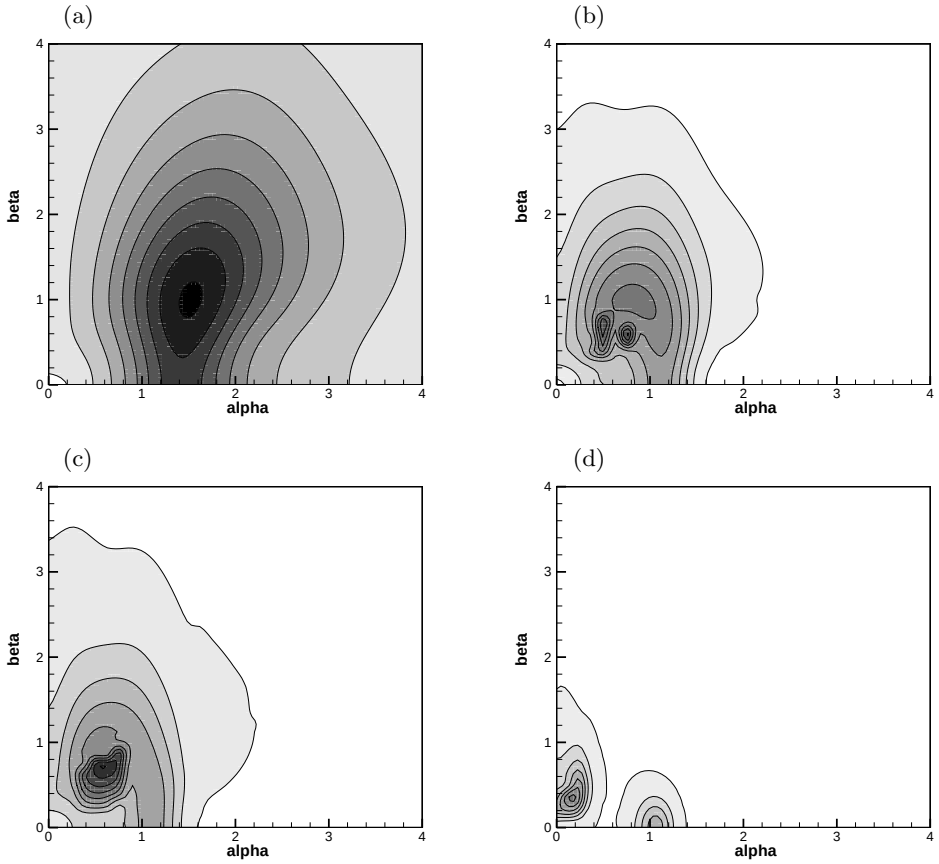

FIGURE 1. Isolevels of energy amplification $\hat{G}(\alpha, \beta)$ in a (α,β)-plane for Reynolds number $Re = 5000$ and Hartmann number $Ha = 50$ at different times T. (a) The $1st$ global maximum at $T = 15$, (b) three local peaks at $T \approx 28$ merging further into (c) the $2nd$ global maximum at $T = 33$ and (d) the $3rd$ global maximum at $T \approx 88$ (also see Fig. 2b).

The motivation for Fig. 3b is to identify possible scaling behavior of the maximum energy amplification with respect to the flow parameters. Such scaling was found in the non-magnetic case, where the maximum amplification of streamwise vortices is proportional to Re^2 (Schmid and Henningson 2001). Our results reveal a pronounced Ha-scaling of the maximum amplification for the streamwise vortices. $\hat{M}_{stream}$ perfectly matches a Ha^{-2} power law starting from $Ha = 5$. We can assume that the scaling is related to the determining role of the magnetic interaction parameter $N = Ha^2/Re$ in the suppression of the streamwise perturbations. The behavior of the global maximal amplification does not show any clear scaling. We also note that the scaling of $\hat{M}_{stream}$ ceases for large Ha since $\hat{M}_{stream}$ is optimized with respect to time T (and thereby necessarily $\hat{M}_{stream} \geq 1$).

4. Non-linear evolution and transition to turbulence

In this Section we study the transition to turbulence triggered by the transient growth of optimal perturbations analyzed in the previous Section. The approach of direct numerical simulations is used, i.e., the non-linear evolution of the flow is found as a numerical

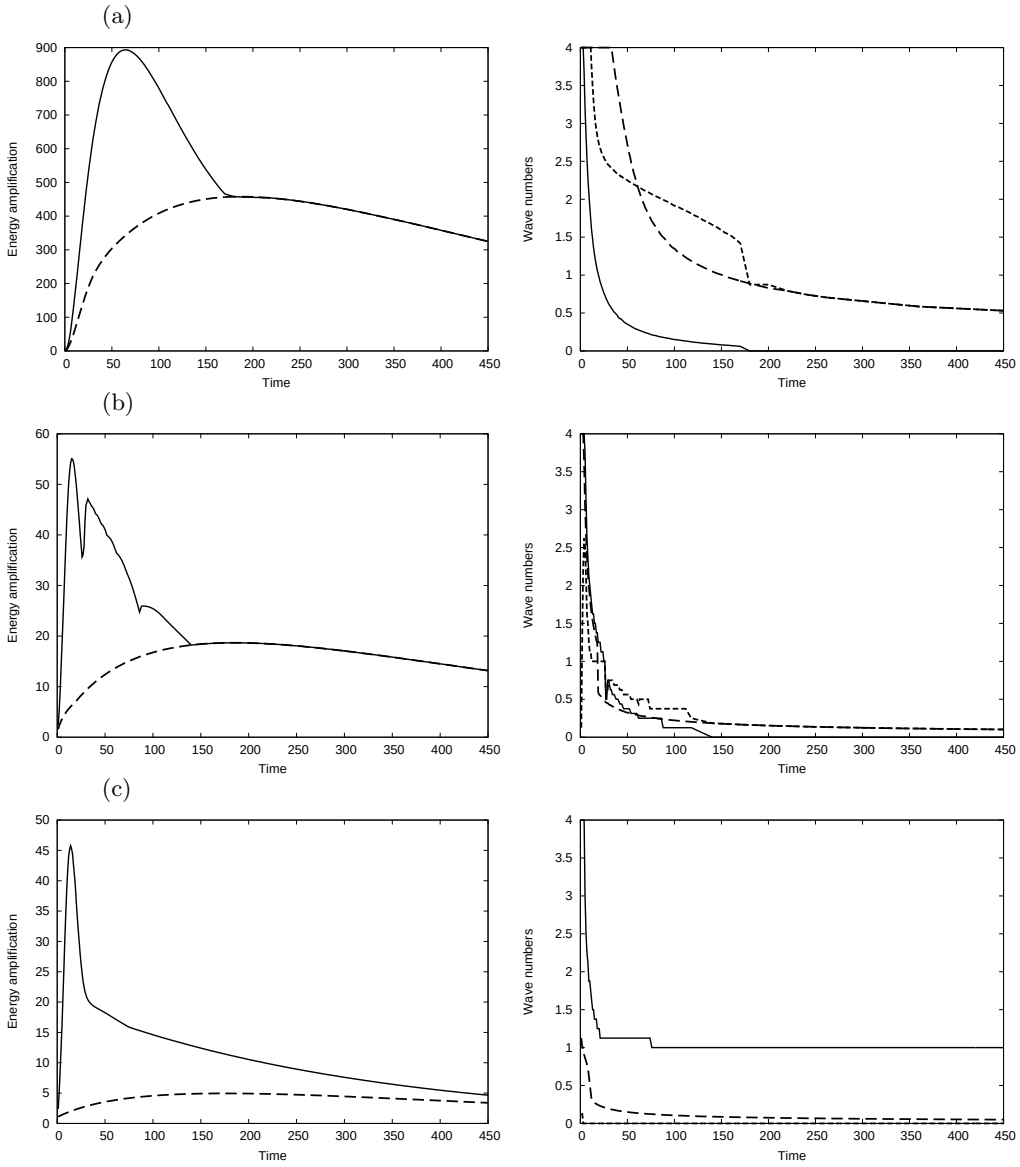

FIGURE 2. (left) Energy amplifications $\hat{M}_{tot}(T, Re, Ha)$ for dominant optimal (———) and $\hat{M}_{stream}(T, Re, Ha)$ for streamwise modes (- - - -) as functions of time T. (right) Dominant optimal wavenumbers α (———), β (-------) at which energy amplification $\hat{M}_{tot}(T, Re, Ha)$ reaches its maximum for given time T and optimal spanwise wavenumber β_{stream} (- - - -) at which energy amplification $\hat{M}_{stream}(T, Re, Ha)$ reaches its maximum for given time T. Results for $Re = 5000$ and Hartmann numbers (a) $Ha = 10$, (b) $Ha = 50$, (c) $Ha = 100$ are shown.

solution of the full equations (2.9)–(2.12). Our pseudospectral method is based on a representation of the flow field by velocity potentials complying with the incompressibility constraint. A detailed description of the algorithm and the corresponding flow solver are given by Krasnov *et al.* (2004). The modifications made for the present work concern the Lorentz force and the time-stepping method. The Lorentz force term is generalized to the

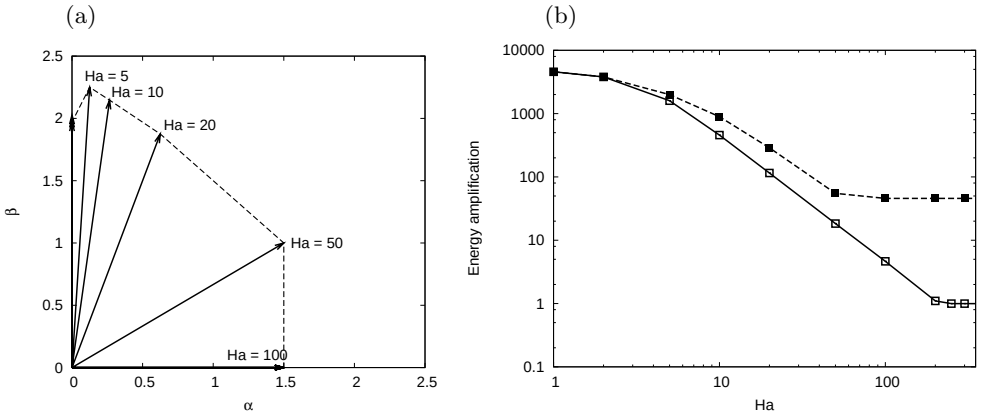

FIGURE 3. (a) Optimal wavevector vs. Hartmann number and (b) amplification gains $\hat{M}_{tot}$ (-------) and $\hat{M}_{stream}$ (———) for global and streamwise optimal modes.

case of arbitrary orientation of the magnetic field and is now treated as an explicit term in the temporal discretization. Furthermore, the new time-stepping scheme uses three time levels for the approximation of the time derivative and is second-order accurate.

All simulations are performed in a domain with a numerical resolution of 128^3 collocation points in the x-, y- and z-directions. The periodicity lengths are specified as $L_x = 2\pi/\alpha_{opt}$ and $L_y = 2\pi/\beta_{opt}$, where α_{opt} and β_{opt} stand for the optimal wavenumbers found in the linear problem. In case of α_{opt} or β_{opt} equal to 0, i.e., purely spanwise or streamwise perturbations, the corresponding periodicity length is set to 2π. We explored the possibility of transition to turbulence in representative flow regimes at $Ha = 10$, 50, and 100. The initial conditions for the runs consist of the basic flow (2.8) modulated by the optimal linear mode of a specified amplitude. The amplitude is chosen so that the kinetic energy of the perturbations $E(0)$ varies between 10^{-5} and 10^{-2} relative to the energy of the basic flow. In the cases where different linear modes give the maximum amplifications at different times (e.g., $Ha = 50$ in Fig. 2b), the simulations are conducted separately for each mode used as initial condition.

One possibility of transition we are particularly interested in is the classical two-step scenario. This scenario implies that the finite-amplitude transient growth is sufficiently strong to render the modulated basic flow unstable to three-dimensional perturbations. In our simulations, the scenario is reproduced by adding weak three-dimensional noise to the modulated flow at the moment $t = t_{opt}$ of maximum linear amplification. The energy E_{3D} of the noise is always chosen to be 10^{-2} of the initial optimal perturbation energy, i.e., $E_{3D}(t_{opt}) = 10^{-2}E(0)$.

In the case of optimal perturbations having the form of oblique rolls, the symmetry of the problem provides an interesting new opportunity. The modes with positive and negative oblique angles of equal magnitude, i.e., with the wavenumbers (α, β) and $(\alpha, -\beta)$ are identical solutions of the linearized equations (2.9–2.12) with the ansatz (3.2) up to the substitution $\hat{v} \to -\hat{v}$ and, thus, have the same linear transient growth properties. However, their nonlinear interaction may lead to faster transition to turbulence than in the case when only one set of rolls is used. In order to verify this hypothesis, additional sets of simulations were performed with initial conditions consisting of two symmetric oblique modes of equal amplitudes (an example is shown in Fig. 4).

For $Ha = 10$, there are two potential candidates for transition, as shown by the

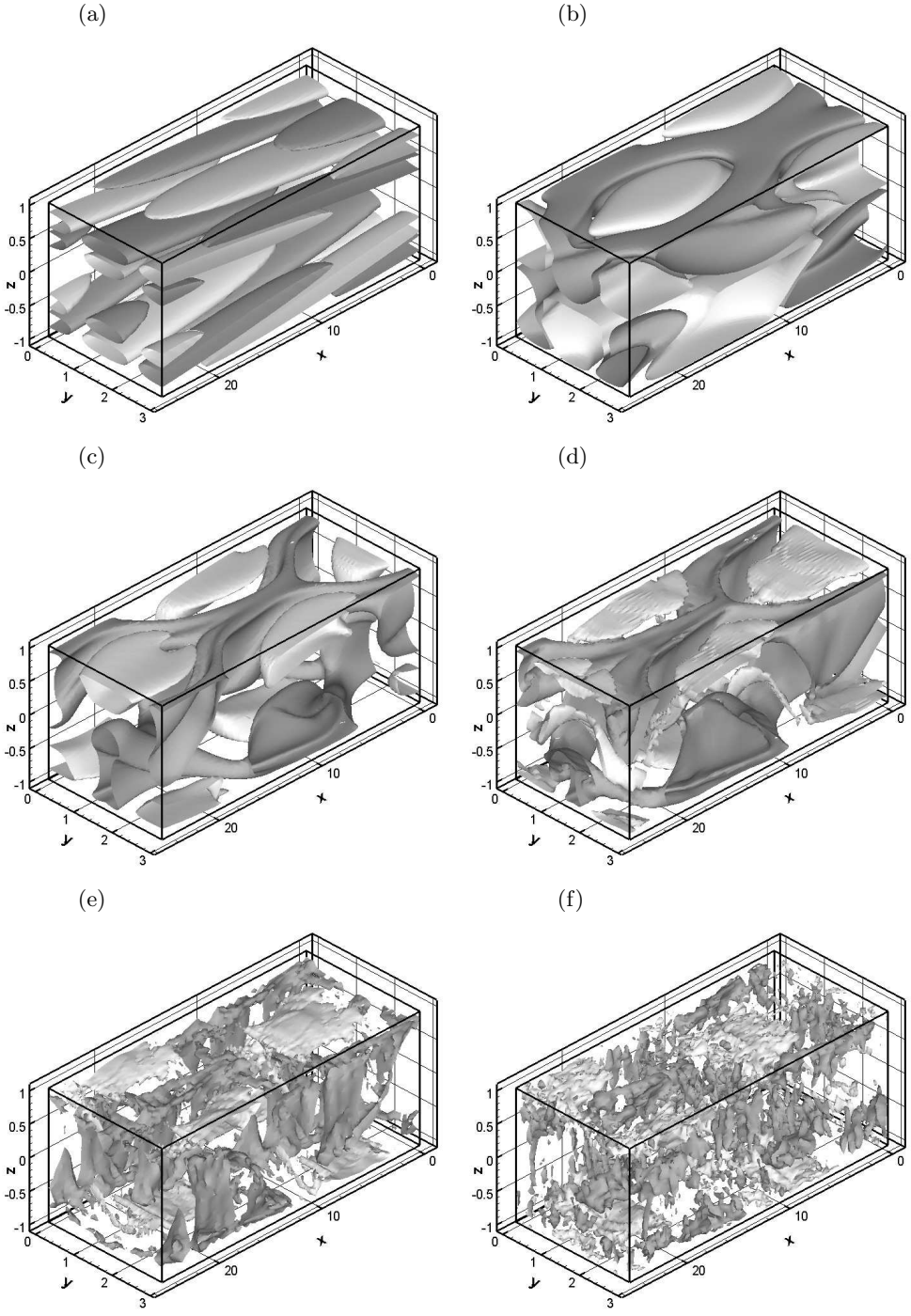

FIGURE 4. Instability and transition to turbulence at $Re = 5000$ and $Ha = 10$ triggered by a superposition of (α, β) and $(\alpha, -\beta)$ optimal perturbations. Six stages of the evolution are visualized by the isosurfaces of the streamwise velocity perturbations.

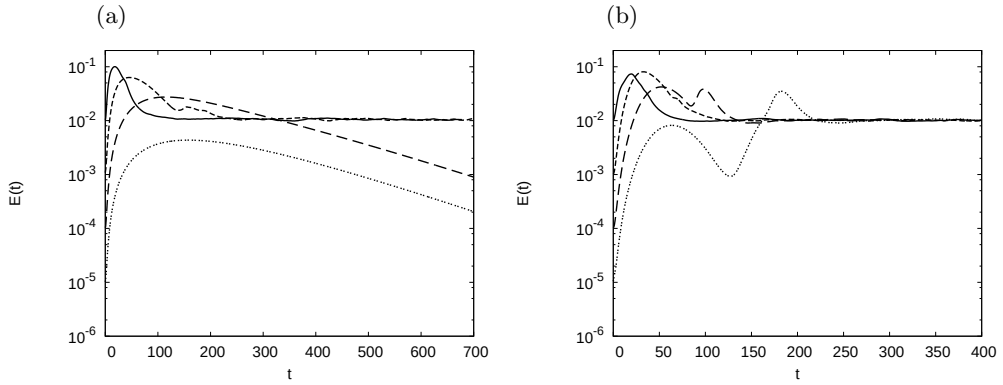

FIGURE 5. The non-linear temporal evolution of energy $E(t)$ and transition to turbulence at $Re = 5000$ and $Ha = 10$ by two different flow modulations: (a) streamwise optimal mode and (b) dominant oblique mode. Initial amplitude for both modes $E(0) = 10^{-2}$ (———), 10^{-3} (-------), 10^{-4} (- - - -) and 10^{-5} (·····); 3D noise $E_{3D} = 10^{-2}E(0)$ added at $t = t_{opt}$ in both cases.

linear results in Fig. 2a: streamwise vortices ($\hat{M}_{stream} \approx 450$) and a dominant mode in the form of oblique rolls ($\hat{M}_{tot} \approx 900$). Both of them were analyzed. The simulations show that for $Ha = 10$ there is already a significant effect of the magnetic field on the streamwise vortices. As Fig. 5(a) depicts, they do not induce transition to turbulence if the perturbation amplitude is less than 10^{-4}. The non-linear evolution of the oblique optimal mode is similar, except that it is a far better candidate to modulate the flow and trigger the transition. Even an initial energy as small as $E(0) = 10^{-5}$ is sufficient for the transition when 3-D noise is added (see Fig. 5(b)). In addition, the transition occurs earlier than in the case of streamwise vortices. Here we also note that, for both purely streamwise and oblique modes, the flow remains laminar if no 3-D noise is present, at least for the range of $E(0)$ values considered.

Analyzing the flow evolution caused by two superimposed oblique waves with (α,β) and (α,$-\beta$), we found transition to turbulence for all $E(0)$ in a range from 10^{-5} to 10^{-2}. The major difference with the 1-wave case was that no 3-D noise had to be added. This confirms the hypothesis that the non-linear interaction of two symmetric waves can be sufficient to destabilize the flow and trigger the transition to turbulence. Thus, this scenario can be considered as "the most optimal," since no additional noise is required. Figure 4 shows a series of intermediate stages for this process, including initial state, interaction between two superimposed modes, lifting-up and breakdown of vortices and, finally, formation of turbulent flow.

For $Ha = 50$ we need to study the non-linear evolution of three oblique optimal modes and of the streamwise mode (see Fig. 2b), each providing the maximum amplification in a certain time range. We have applied the same types of flow excitation as before, i.e., "single mode + 3D noise," "superposition of symmetric oblique modes," and, additionally, "superposition of symmetric oblique modes + 3D noise." The simulations have shown that non-linear effects become noticeable when the initial perturbation energy is $E(0) \geq 10^{-3}$. Despite that, none of these types of perturbations can trigger the transition to turbulence. One reason for the flow being so stable is that the maximum energy amplification is only 55 for the $1st$ mode, and even lower for the others. Another plausible explanation of the observed re-laminarization is proposed below based on the case $Ha = 100$.

The situation at $Ha = 100$ differs from the previous cases. There is only one dom-

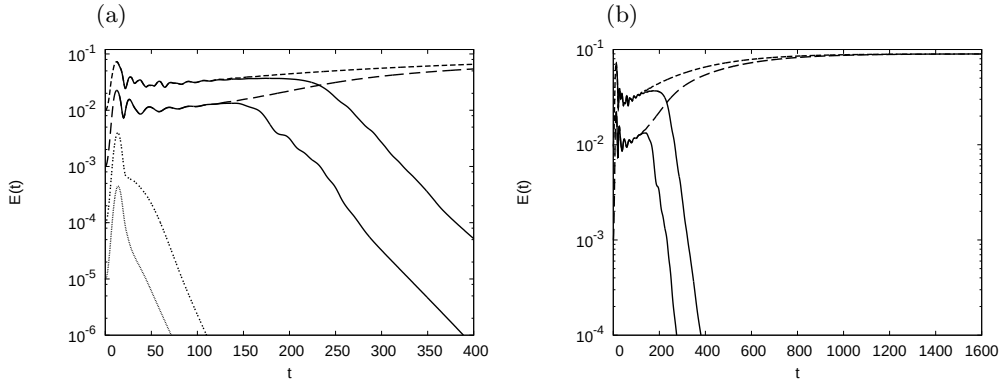

FIGURE 6. The non-linear temporal evolution of energy $E(t)$ starting with the dominant optimal mode at $Re = 5000$ and $Ha = 100$. Initial amplitude of this mode is $E(0) = 10^{-2}$ (-------), 10^{-3} (- - - -), 10^{-4} (·····), 10^{-5} (·····) without the 3-D noise. The solid lines (———) show the evolution of the flows with 3-D noise $E_{3D} = 10^{-2}E(0)$ added at $t = t_{opt}$. The early stage (a) in detail and the complete evolution up to a sustained 2-D-oscillating state (b) for $E(0) = 10^{-2}$ and 10^{-3} are shown.

inant mode. When the dominant mode alone is imposed (no noise), sufficiently strong perturbations (e.g., $E(0) \geq 10^{-3}$ in Fig. 6) evolve into a purely two-dimensional finite-amplitude state characterized by oscillations observed earlier by Jimenez (1990) for a two-dimensional non-magnetic channel flow. This is not surprising, as the dominant mode has the form of purely spanwise vortices, which are unaffected by the spanwise magnetic field. Therefore, this evolution can be regarded as a common solution for all values of Ha, including the non-magnetic case. If 3-D noise is added at $t = t_{opt}$ in the non-magnetic case, it triggers the transition to a 3-D turbulent state. Contrary to that, the noise destroys the time-dependent two-dimensional flow for $Ha = 100$ in such a way that it returns back to the laminar regime as illustrated in Fig. 6 (bold curves). We attribute this re-laminarization to energy transfer from the 2-D modes to modes with a finite spanwise wavenumber, which are rapidly damped by Joule dissipation. We varied the amplitude E_{3D} and found that even very small noise with $E_{3D}(t_{opt}) = 10^{-20}E(0)$ (comparable with the round-off error of floating-point operations) is sufficient to trigger the re-laminarization. We have also carried out a series of similar simulations for $Ha = 50$ and found almost the same re-laminarization behavior as at $Ha = 100$.

We can, therefore, conclude that, whereas a sufficiently strong magnetic field (e.g., $Ha \geq 50$ for $Re = 5000$) eventually suppresses any three-dimensionality in the flow, it cannot sustain the non-steady two-dimensional solutions found by Jimenez (1990).

5. Conclusions

The transient growth of linear perturbations in a laminar channel flow is suppressed by a spanwise magnetic field, and the optimal perturbations change from streamwise rolls to oblique rolls. The oblique angle of the optimal modes increases monotonically with the magnetic field strength until the spanwise Tollmien-Schlichting vortices unaffected by the magnetic field become the modes with strongest transient amplification. In comparison with a single optimal oblique mode, the transition to turbulence occurs at lower perturbation amplitudes when a combination of two symmetric oblique modes is used. Sufficiently strong magnetic fields eventually results in the spanwise Tollmien-Schlichting vortices be-

coming the dominant perturbations with strongest transient growth, but cannot stabilize the resulting two-dimensional finite-amplitude solutions, which disintegrate leading to relaminarization of the flow in the presence of even very weak three-dimensional noise.

Acknowledgments

The authors are grateful to Prof. Parviz Moin and the staff of the Center for Turbulence Research for their hospitality during the 2006 summer program. TB and DK acknowledge support by the Deutsche Forschungsgemeinschaft (Grant Bo1668/2-2). OZ acknowledges support from the U.S. Department of Energy (Grant DE FG02 03 ER46062). The cooperation between the University of Michigan – Dearborn and the Technische Universität Ilmenau is supported by the U.S. National Science Foundation (Grant INT 0338713) and DAAD.

REFERENCES

von Ammon, W., Gelfgat, Y., Gorbunov, L., Muhlbauer, A., Muiznieks, A., Makarov, Y., Virbulis, J. & Muller, G. 2005 Application of magnetic fields in industrial growth of silicon single crystals. In *The* 15^{th} *Riga and* 6^{th} *PAMIR Conference on Fundamental and Applied MHD Modeling of MHD turbulence*, vol. I, pp. 41–54. Riga, Latvia.

Barleon, L., Burr, U., Mack, K. J. & Stieglitz, R. 2001 Magnetohydrodynamic heat transfer research related to the design of fusion blankets. *Fusion Techn.* **39(2)**, 127–156.

Butler, K. M. & Farrell, B. F. 1992 Three-dimensional optimal perturbations in viscous shear flow. *Phys. Fluids A* **4** (8), 1637–1650.

Davidson, P. A. 1999 Magnetohydrodynamics in materials processing. *Annu. Rev. Fluid Mech.* **31**, 273–300.

Farrell, B. F. & Ioannou, P. J. 1996 Generalized stability theory part I: autonomous operators. *J. Atmos. Sci.* **53**, 2025–2040.

Jimenez, J. 1990 Transition to turbulence in two-dimensional Poiseuille flow. *J. Fluid Mech.* **218**, 265–297.

Krasnov, D. S., Zienicke, E., Zikanov, O., Boeck, T. & Thess, A. 2004 Numerical study of instability and transition to turbulence in the Hartmann flow. *J. Fluid Mech.* **504**, 183–211.

Lee, D. & Choi, H. 2001 Magnetohydrodynamic turbulent flow in a channel at low magnetic Reynolds number. *J. Fluid Mech.* **439**, 367–394.

Reddy, S. C., Schmid, P. J., Bagget, P. & Henningson, D. S. 1998 On the stability of streamwise streaks and transition thresholds in plane channel flow. *J. Fluid Mech.* **365**, 269–303.

Roberts, P. H. 1967 *An introduction to Magnetohydrodynamics*. New York: Longmans, Green.

Schmid, P. J. & Henningson, D. S. 2001 *Stability and Transition in Shear Flows*. Springer Verlag.

Thomas, B. G. & Zhang, L. 2001 Mathematical modeling of fluid flow in continuous casting: a review. *ISIJ Intern* **41** (10), 1181–1193.

Zikanov, O. 1996 On the instability of pipe Poiseuille flow. *Phys. Fluids* **8**, 2923–2932.